The effect of H_2 treatment at 423–573 K on the structure and synergistic activity of Pd–Cu alloy catalysts for low-temperature CO oxidation

S.A. Nikolaev *, E.V. Golubina, M.I. Shilina

Faculty of Chemistry, Moscow State University, Leninskie Gory 1, Moscow, 119991, Russia

ABSTRACT

The effect of H_2 treatment at 423–573 K on the structure of $Cu/Pd/Al_2O_3$ catalysts for low-temperature CO oxidation was studied by means of XRD, TEM, EDS, FFT, DRIFTS, and XPS methods. The formation of 5 nm alloy particles in the Cu/Pd catalyst reduced at 423 K was detected. The reaction on Cu/Pd, Pd, and Cu catalyst reduced at 423 K starts at 275, 400, and 475 K, respectively. The activation energy for CO oxidation on Cu/Pd, Pd, and Cu catalyst is 30, 90, and 110 kJ/mol, respectively. The enhanced activity of Cu/Pd catalyst is explained by oxidation on Pd^0–MO_x interfaces (M = Pd, Cu). The key steps of this process are: oxidation of CO molecules strongly bound to Pd^0 by lattice oxygen of MO_x; fast desorption of CO_2 molecules; replenishment of oxygen vacancies in MO_x by oxygen molecules from reaction media. As a result, a substantial part of "blocked" Pd^0 sites become available for adsorption and dissociation of O_2 molecules. This is favorable for low-temperature oxidation via Langmuir–Hinshelwood mechanism. The increase in the reduction temperature results in a separation of alloy particles into metallic particles. As a result, Cu/Pd catalysts reduced at high temperatures are characterized with a decreased content of Pd^0–MO_x interfaces; an essential amount of "blocked" Pd^0 sites and a decreased light-off activity.

© 2017 Elsevier B.V. All rights reserved.

1. Introduction

Catalytic CO oxidation has received attention due to its application in automotive exhaust gas after-treatment [1,2]. Commercial Pt–Pd–Rh catalysts, used for this process [3], convert CO to CO_2 in nearly 100% yield once they reach the high temperature, typically above 673 K. The time needed to reach this temperature after the internal combustion engine has been switched on is 3–10 min. During this period, Pt–Pd–Rh catalysts do not provide 100% conversion of CO, which is, hence, discharged to the atmosphere. Thus, developing of new catalysts able to oxidize CO at low temperature is still an important task.

The modification of a monometallic catalyst (M_1/support) by a second metal (M_2) can significantly enhance the catalytic activity of the M_1/support catalyst [4–13]. Sometimes this modification results in a 10- to 1000-fold increase in the activity of an M_1–M_2 catalyst in comparison with the sum of activities of monometallic analogs (M_1/support and M_2/support). In that case, M_1–M_2 catalysts are called synergistic [7].

It is possible to distinguish three groups of synergistic catalysts with high potential for the low-temperature CO oxidation. The catalysts of the first group are gold clusters promoted with oxides of non-noble metals: Au–Cu, Au–Ce, Au–Ni, Au–Mn, Au–Fe, Au–Zn, etc. For example, Liu et al. reported that SBA-15-supported Au–Cu, Au, and Cu catalysts oxidize 80, 36, and 0% of CO at 300 K, respectively [14]. Centeno et al. reported that Al_2O_3-supported Au–Ce, Au, and Ce catalysts oxidize 89, 2, and 0% of CO at 310 K, respectively [15]. Grisel et al. had studied the activity of Au–MO_x/Al_2O_3, Au/Al_2O_3, and MO_x/Al_2O_3 (M = Cr, Mn, Fe, Co, Ni, and Zn) catalysts. They found that all multi-component catalysts show a remarkable enhancement of the low-temperature CO oxidation compared with the mono-component catalysts and that the activity of Au–MO_x/Al_2O_3 toward CO oxidation varies in the series: Mn > Ni > Zn > Fe > Co > Cr [4,5]. The high activity of Au–M_2 catalysts is usually attributed to the presence of small (3–4 nm) Au particles anchored to the M_2 phase [1,4,5,10].

An industrial application requires a catalyst to show not only a high activity but also a long lifetime. In this respect, Au–M_2 catalysts often have a problem due to segregation of metals [3]. The high cost price of gold also limits a wide application of Au–M_2 catalysts [3].

* Corresponding author at: Faculty of Chemistry, Moscow State University, Leninskie Gory 1, Moscow 119991, Russia. Tel.: +7 4959393498; fax: +7 4959328846.
E-mail address: serge2000@rambler.ru (S.A. Nikolaev).

The synergistic catalysts of the second group are mixed oxides of non-noble metals: Co–Ce, Cu–Ce, Fe–Ce, Mn–Sn, Cu–Ni, etc. [16]. These catalysts are not very expensive and sometimes possess good time-on-stream performance. For example, Hou et al. reported that the CO conversion on CeO_2/Co_3O_4 catalysts at 400 K remains 100% for 140 h, whereas a physical mixture of Co_3O_4 and CeO_2 shows 0.1% CO conversion after 2 h [17]. Lou et al. reported that the modification of Co_3O_4 by Bi_2O_3 (20 wt%) or In_2O_3 (25 wt%) significantly enhances its catalytic performance: CO oxidation activity of Bi_2O_3/Co_3O_4 and In_2O_3/Co_3O_4 catalysts remains constant for at least 10 h and they oxidize 100% of CO even at 150–170 K [18–20]. The reaction rate in the presence of Bi_2O_3/Co_3O_4, In_2O_3/Co_3O_4, Co_3O_4, Bi_2O_3, and In_2O_3 equals 17, 15, 4, < 0.1 and < 0.1 $\mu mol(CO) \times g(catalyst)^{-1} \times s^{-1}$, respectively [18–20]. This indicates a synergy of catalytic action between Co_3O_4 and dopant oxide. The enhanced activity of M_1O_x/M_2O_y catalysts is usually attributed to the interaction between M_1O_x and M_2O_y species, resulting in an increase in the oxygen storage capacity of the surface [7–9,16].

The third group of synergistic catalysts suitable for low-temperature CO oxidation includes highly active Pd, Pt, and Rh catalysts promoted with non-noble metal species: Pt–Cu, Pt–Ni, Rh–Cu, Pd–Ag, Pt–Ag, Pd–Cu, etc. [8,9]. The cost price of Pd is lower in comparison with Pt or Rh, which makes Pd–M_2 catalysts most attractive from the economic point of view. The synergistic Pd–Cu nanocomposites for CO oxidation have been vigorously studied in the last decades. It was revealed that the catalytic performance of these catalysts is dependent on several parameters, such as the preparation method, type of the support, Pd to Cu ratio, and the oxidation states of the metals. The main results of these studies are summarized below.

Choi et al. reported that the TOF at 300 K for carbon-supported $PdCl_2$–$CuCl_2$, $PdCl_2$, and $CuCl_2$ species is 2.2×10^{-2}, 1×10^{-4}, and 1×10^{-7} s^{-1}, respectively [21,22]. Wang et al. suggested that the presence of $Cu_2Cl(OH)_3$ accelerates the re-oxidation of Pd^0 to Pd^{2+} in the supported $PdCl_2$–$CuCl_2$ catalysts, which results in increase in the CO oxidation rate [23,24]. $PdCl_2$–$CuCl_2$ species supported on Al_2O_3 possess better performance than those on TiO_2 [23]. The CO conversion is maintained at about 30% with the $PdCl_2$–$CuCl_2/Al_2O_3$ catalyst for 45 h, while it rapidly decreases from 20 to 1% with the $PdCl_2$–$CuCl_2/TiO_2$ catalyst at 286 K. It was suggested that the larger surface area of Al_2O_3 facilitates the dispersion and stabilization of active Pd species. Shen et al. reported that the Pd–Cu catalyst prepared by conventional impregnation is less active and is rapidly deactivated, while the Pd–Cu catalyst prepared by coordination impregnation shows higher activity and stability [25,26]. A theoretical study of Tang et al. on the catalytic activity of Pd–Cu alloys for oxygen reduction predicted that Cu would decrease the Pd–O binding energy, whereas Pd would increase the Cu–O binding energy, as a result of charge transfer from Pd to Cu [27]. It was also found that the activity of Pd–Cu nanoalloys would peak at a Pd:Cu ratio of 50:50 [27]. Shan et al. confirmed this prediction by CO oxidation on Pd–Cu alloys prepared from Pd and Cu acetylacetonates [28]. Wang et al. reported that the nature of Cu precursors is crucial for Pd–Cu/Al_2O_3 catalysts: the activity toward CO oxidation varies in the series: $CuCl_2 \approx Cu(NO_3)_2 > Cu(acac)_2 > CuSO_4$ [29]. This result was explained by different degrees of dispersion of the active phase. Estifaee et al. studied the effect of Pd loading in Pd–Cu/Al_2O_3 catalysts prepared by sonochemical method [30]: it was reported that Pd (1.5%)–Cu (20%)/Al_2O_3 has the best performance in CO oxidation. Di et al. compared CO oxidation activity of Pd/Al_2O_3 and Pd–Cu/Al_2O_3 catalysts prepared by the thermal reduction and cold plasma methods. The detected synergistic effect was attributed to specific features of Pd–Cu catalysts: the formation of Pd–Cu particles with high alloying degree, smaller particle size, and a higher Pd^0 to Cu^+ ratio [2].

Despite the excellent theoretical and experimental studies mentioned above, the effect of reduction temperature on the structure of synergistic Pd–Cu catalysts for low-temperature CO oxidation has been studied poorly. To the best of our knowledge, there is only one study concerning the effect of reduction temperature on the structure and activity of Pd–Cu particles prepared from colloidal solutions and deposited on TiO_2, CeO_2, SiO_2, and C [28]. Note that such studies are crucial for preparation of highly active catalysts, because the conditions of reductive treatment have a pronounced effect on the morphology and electronic features of supported phases, and determine the activity of M_1–M_2 catalysts in redox processes [4,5,8–12].

In this study, our team concentrated the effort on elucidation of the effect of reduction temperature on the structure of synergistic Pd–Cu catalysts for low-temperature CO oxidation. A model Cu/Pd/Al_2O_3 catalyst with equimolar Cu:Pd ratio and its monometallic analogs were prepared from nitric precursors by deposition–precipitation and impregnation. The chosen methods are simple and can be easily scaled to industrial production of the catalysts. The support was chosen because of its large specific surface and inertness in CO oxidation under the experimental conditions of the current study. The mono- and bimetallic catalysts were reduced with hydrogen at 423–573 K and their light-off activity was measured in the CO oxidation at 273–723 K. The catalyst structure was studied by means of X-ray diffraction (XRD), transmission electron microscopy (TEM), energy dispersive X-ray spectroscopy (EDS), electron diffraction simulation by fast Fourier transformation (FFT) procedure, diffuse reflectance infrared Fourier transform spectroscopy (DRIFTS), and X-ray photoelectron spectroscopy (XPS). The evolution of the catalysts surface during reductive treatment and its impact on the activity was studied and discussed. The possible explanation for enhanced activity of Cu/Pd catalyst was also proposed and discussed.

2. Experimental

2.1. Catalyst preparation

γ-Al_2O_3 (Catalyst LLC, S = 160 m^2/g) calcined at 723 K for 3 h, $Cu(NO_3)_2 \times 6H_2O$ (Sigma-Aldrich, 98% pure), and $Pd(NO_3)_2 \times 2H_2O$ (Sigma-Aldrich, 40 wt% Pd) were used.

Monometallic Cu catalysts were prepared by impregnation [31,32]. In a typical procedure, 5 g of Al_2O_3 was added to 5.5 mL of an aqueous solution of $Cu(NO_3)_2 \times 6H_2O$ containing 3×10^{-4} mol of copper, and the solid was dried at 300 K for 24 h and calcined at 423 K for 4 h. Then 2.5 g of the calcined solid was reduced with H_2 at 423 K for 4 h and designated as Cu (423) catalyst, the remaining solid (2.5 g) was reduced at 473 K for 4 h and designated as Cu (473) catalyst.

Monometallic Pd catalysts were prepared by deposition–precipitation [33]. In a typical procedure, $Pd(NO_3)_2 \times 2H_2O$ (0.16 g, i.e., 6×10^{-4} mol of Pd) was dissolved in 50 mL of water, the pH of the solution was adjusted to 7.0 by addition of 0.1 M NaOH, 10 g of Al_2O_3 was added to the solution, the resulting suspension was stirred at 343 K for 1 h, and the solid was separated, washed with 5 L of hot water, dried at 300 K for 24 h, and calcined at 423 K for 4 h. Then 1 g of calcined Pd-containing solid was reduced with H_2 at 423 K for 4 h and designated as Pd (423) catalyst, another 1 g of calcined Pd-containing solid was reduced at 473 K for 4 h and designated as Pd (473) catalyst.

Unreduced Cu/Pd (423)* catalyst was prepared by impregnation using 1 g of calcined Pd-containing solid (see synthesis of monometallic Pd catalyst) and 1.1 mL of an aqueous solution containing 6×10^{-5} mol of copper. After the impregnation step, Cu/Pd

(423)* catalyst was dried at 300 K for 24 h and calcined at 423 K for 4 h.

Reduced Cu/Pd (423), Cu/Pd (473), Cu/Pd (523), and Cu/Pd (573) catalysts were prepared by impregnation using 1 g of calcined Pd-containing solid and 1.1 mL of an aqueous solution containing 6×10^{-5} mol of copper. After the impregnation, Cu/Pd (423), Cu/Pd (473), Cu/Pd (523), and Cu/Pd (573) catalysts were dried at 300 K for 24 h and reduced for 4 h with H_2 at 423, 473, 523, and 573 K, respectively. Between experiments, the prepared catalysts were kept in a box filled with dry argon.

The metal content in Cu, Pd, and Cu/Pd catalysts was determined by atomic absorption spectroscopy (AAS) on a Thermo iCE 3000 AA spectrometer. A catalyst (0.1 g) was treated with 10 mL of aqua regia ($HCl:HNO_3 = 4:1$) for 1 h. This mixture was added to 90 mL of H_2O. The metal content in the solution was measured by AAS with application of the calibration curves [34]. The actual metal content in the catalyst [C_1] was calculated as $[C_1] = [C_2] \times 100\,mL \times 0.1\,g^{-1} \times 100\%$, where [$C_2$] is the metal content in 100 mL of the solution measured by AAS. The actual metal content in the catalysts was 0.37 ± 0.03 wt% (Cu) and 0.64 ± 0.02 wt% (Pd). These values correspond to the desired equimolar Cu:Pd ratio.

2.2. Catalyst characterization

XRD analysis was carried out on a Bruker D8 advance diffractometer with Ni-filtered CuKα radiation and LYNXEYE detector. The samples were prepared by mechanical dispersion of the catalysts. The diffraction data were collected in the 2θ range from 20 to 80° with a step of 0.02°.

TEM analysis was carried out on a JEOL JEM-2100F/UHR microscope. The samples were prepared by ultrasonic dispersion of the catalysts (0.2 g) in ethanol (10 mL) followed by deposition of a drop of the suspension on a carbon-coated Ni grid. The assignment of dark spots visible in TEM images to metal particles was performed by local EDS analysis with application of a JED-2300 X-ray spectrometer. The size of a single particle was calculated as the maximum linear dimension. For each catalyst, 300–380 particles were processed to determine the particle size distribution.

The lattice d-spacing values were calculated from the fast Fourier transformation (FFT) patterns for planes visible in high-resolution TEM images (HRTEM). The assignment of a d-spacing to a certain plane on the surface of the particles was verified by the distance ratios and angles for the face-centered cubic (FCC) structure of different Cu and Pd species. The relative content of individual and alloy particles in Cu/Pd catalysts was determined from TEM-EDS mapping with application of FFT analysis of HRTEM images of bimetallic particles. Ten random areas (100×100 nm) were processed for each Cu/Pd catalyst.

XPS analysis of the catalysts was performed on a Kratos Axis Ultra DLD spectrometer using Al Kα radiation (1486.6 eV). The binding energies were corrected by referencing to the internal standard – Al 2p (74.6 eV). XPS spectra were normalized to the Al 2p line intensity. Decomposition of Cu $2p_{3/2}$ peak into ($Cu^0 + Cu^+$) and (Cu^{2+}) components was performed with the Shirley background, GL (30) line shapes, and binding energies for nano-sized Cu species supported on alumina [2]. The Cu $2p_{3/2}$ peak area for Cu^{2+} species was calculated from the area of Cu^{2+} shake-up satellite as described by Biesinger et al. [35]. Decomposition of Pd 3 d peaks into (Pd^0) and (Pd^{2+}) components was performed with the Shirley background, GL (30) line shapes, and binding energies for nano-sized Pd species supported on alumina [2,36,37].

The DRIFT spectra of adsorbed CO for catalysts were recorded using an InfraLUM FT-801 spectrometer equipped with a diffuse-reflectance attachment with $4\,cm^{-1}$ resolution in the range from 900 to $6000\,cm^{-1}$. Accumulation of 128 scans was used for collect-

ing each spectrum. The spectra were converted into Kubelka–Munk units. In a typical experiment, 0.04 g of a catalyst was loaded into the DRIFT cell and heated in vacuum at 473 K for 2 h. The cell was cooled to 298 K and then a background spectrum (A) was recorded. The equilibrium CO pressure (0.2 kPa) was added to the sample at 298 K and then a spectrum (B) was recorded. The final spectrum was obtained by subtracting spectrum A from spectrum B.

2.3. CO oxidation

The reaction was carried out under atmospheric pressure in a quartz reactor in a pulse mode [1,38]. With this approach, a significant modification of the catalysts by the reactants is avoided, resulting in more reliable correlations between the catalytic performance and the sample structure. Helium at a total flow rate of 70 mL/min (gas hourly space velocity: $46\,700\,h^{-1}$) was passed through the reactor during the experiments. A gas mixture (2% CO + 1% O_2 + 97% He) was introduced as the reactants. In a typical experiment, 0.1 g of a catalyst was loaded into the reactor and heated to the desired temperature (T). A pulse of reactants (1 mL) was injected into the reactor. The flow compositions at the reactor inlet and outlet were determined by GC on an LHM-80 gas chromatograph equipped with a thermal conductivity detector and a packed column (Porapak Q, 1 m, id 2 mm). CO conversion was calculated from CO and CO_2 peak areas using pre-constructed calibration curves. Ten to thirty pulses were injected in order to obtain steady-state CO conversion value α at each temperature. These values were used to elucidate the dependence of α on the reaction temperature. The light-off catalytic activity was determined as T_{10} (the temperature at 10% α).

3. Results and discussion

The main goal of this study was to reveal the effect of reduction temperature on the structure and synergistic activity of Cu/Pd catalysts for low-temperature CO oxidation. According to this goal, each bimetallic sample was characterized by XRD, TEM, EDS, FFT, and XPS method. The monometallic analogs of the best bimetallic catalysts (Cu/Pd (423) and Cu/Pd (473)) were prepared and analyzed by the same set of methods. The results of the structural and catalytic studies are presented and discussed below.

3.1. XRD measurements

The XRD patterns of the support and reduced Cu (423), Pd (423), and Cu/Pd (423) catalysts are presented in Fig. S1. Diffraction peaks at 2 θ of 32.4, 37.5, 39.5, 46.0, 61.1, and 66.8° are observed for the support. These peaks are assignable to (220), (311), (222), (400), (511), and (440) planes of γ-Al_2O_3 (JCPDS card No.29 − 0063). The similar peaks are observed for Cu (423), Pd (423), and Cu/Pd (423) catalysts (Fig. S1). No peaks of Cu or Pd species were found for these (and other) catalysts of this study. The absence of peaks in the XRD patterns of nanocomposites is a rather typical situation and could be explained by the high dispersion and/or relatively low metal content in the catalysts [1,12,13].

3.2. TEM, EDS, and FFT measurements

3.2.1. Morphological features of Cu and Pd catalysts

Dark spherical spots can be seen in the TEM images of the reduced Cu (423) catalyst (Fig. 1(a) and (b)). The EDS spectrum of these spots exhibits peaks corresponding to C, Ni, Al, O, and Cu elements (Fig. S2(a)). Ni and C elements are attributable to the TEM grid and should not be taken into consideration. The rest combination of elements indicates that the dark spots seen in the TEM images are due to copper particles deposited on alumina surface.
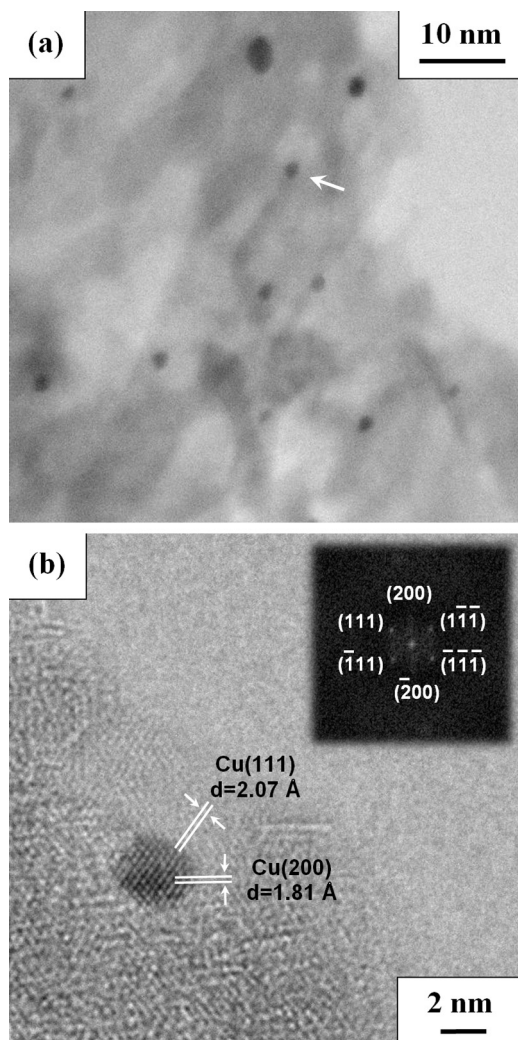
Fig. 1. (a) TEM image of the particles in the Cu catalyst reduced at 423 K; (b) HRTEM image of the Cu particle selected on TEM image and FFT patterns of this particle.

Fig. 2. (a) TEM image of the particles in the Pd catalyst reduced at 423 K; (b) HRTEM image of the Pd particle selected on TEM image and FFT pattern of this particle.

The structure of Cu (423) catalyst single particles can be indexed as an FCC structure, as depicted in the inset of FFT patterns in Fig. 1(b). The lattice spacings of 1.81 and 2.07 Å correspond to Cu (200) and Cu (111) planes, which are visible on the particle surface (Fig. 1(b)).

The FCC lattice constant (a) was calculated as: $a = d(hkl) \times (h^2 + k^2 + l^2)^{1/2}$, where a is the FCC lattice constant; h, k, l are the Miller indices for the Cu (111) plane; d is the lattice spacing for Cu (111) plane measured from the FFT patterns. The calculated lattice constant is 3.52 Å, which is close to that of metallic copper (3.61 Å). The size of the detected particles in the Cu (423) catalyst is 1–8 nm, and the average size is 4 nm (Fig. S2(b)). The hydrogen reduction of Cu catalyst at 473 K does not change the spherical shape, FCC structure, or lattice parameters of the particles. Only a slight increase in the average particle size by 0.5 nm can be observed for the Cu (473) catalyst in comparison with Cu (423) (Fig. S2(b)).

TEM images of the reduced Pd (423) catalyst contain dark spherical spots (Fig. 2(a) and (b)). According to the EDS spectrum of these spots, they can be attributable to palladium particles deposited on alumina (Fig. S3(a)). The structure of a palladium particle in Pd (423) catalyst can be indexed as FCC (FFT patterns in Fig. 2(b)). The lattice spacings of 1.94 and 2.25 Å correspond to Pd (200) and Pd (111) planes, which are visible on the particle surface (Fig. 2(b)). The calculated FCC lattice constant is 3.89 Å, which corresponds to metallic
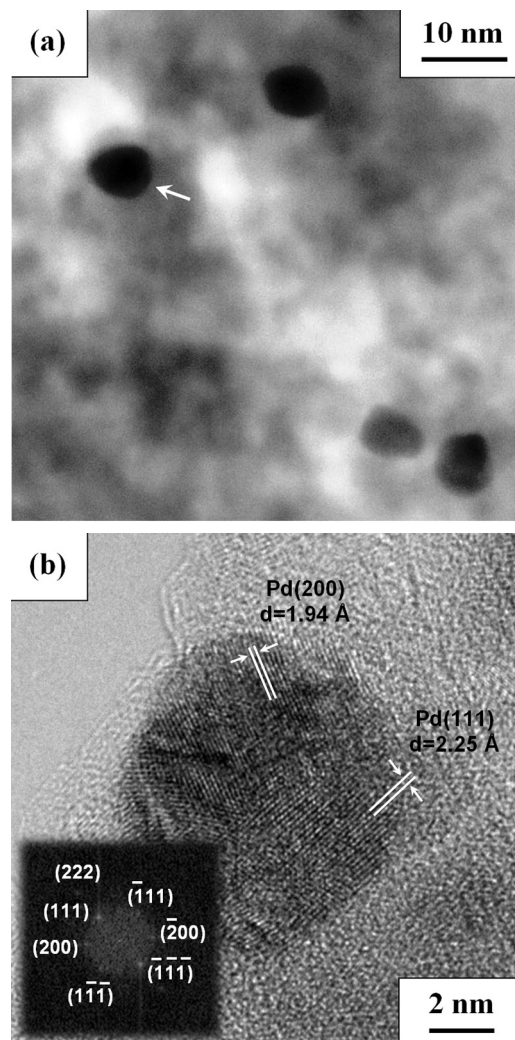
palladium (a = 3.89 Å). The size of the detected particles in Pd (423) catalyst is 1–24 nm, and the average size is 8 nm (Fig. S3(b)). Reduction at 473 K does not change the spherical shape, FCC structure, or lattice parameters of Pd (473) catalyst particles, but it results in a significant increase in the average particles size by 6 nm (Fig. S3(b)). The increase in the average particle size can be explained by aggregation of the reduced palladium particles during calcination of the catalysts as reported in Refs. [6–9].

3.2.2. Morphological features of Cu/Pd catalysts

The TEM–EDS mapping of a large area of unreduced Cu/Pd (423)* catalyst is presented in Fig. 3(a) – (c). They demonstrate the deposition of copper over palladium species. The EDS spectrum of the particle selected in the HRTEM image indicates that the Pd:Cu ratio in this particle is 50 at%:50 at% (Fig. 3(d) and (e)). Some planes on the surface of this particle are attributable to individual CuO (111) and PdO (111) planes with lattice spacings of 2.45 and 3.25 Å (Fig. 3(d) and (f)). These results indicate that Cu/Pd particles in the Cu/Pd (423)* catalyst consists of individual CuO and PdO phases. The particle size in the Cu/Pd (423)* catalyst is 1–18 nm, and the average size is 4 nm (Fig. S4(a)).

The morphological features of reduced Cu/Pd catalysts are shown in Figs. 4–6, S4, S5, and in Table 1. There are many particles with irregular shape and average size of 5 nm on the Cu/Pd (423)
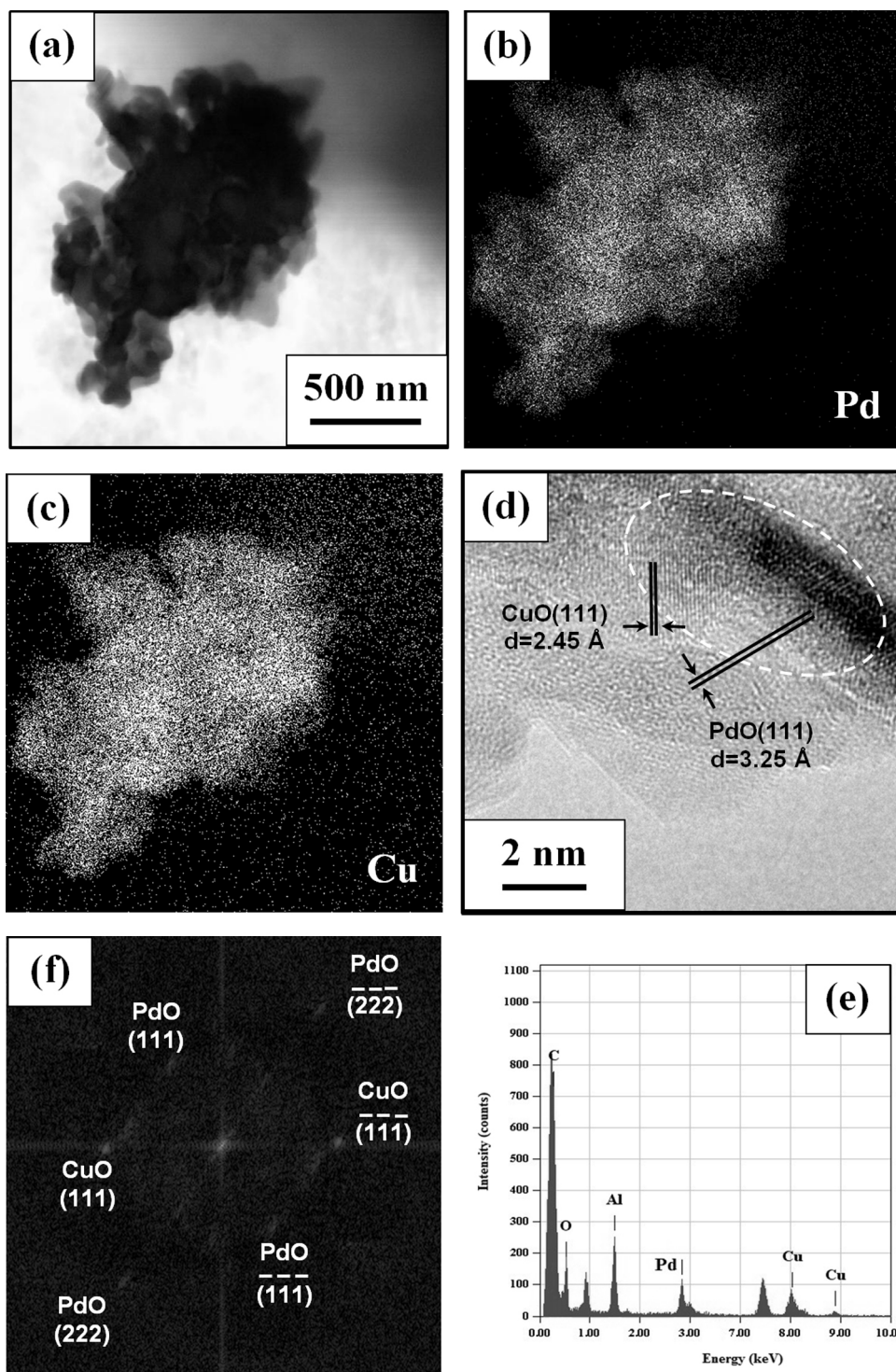
Fig. 3. (a) TEM image of the unreduced Cu/Pd catalyst; (b) and (c) distribution of Pd *L* and Cu *K* signal over the surface of this catalyst; (d) and (e) HRTEM image and EDS spectrum of individual bimetallic particle; (f) FFT patterns of this bimetallic particle.

catalyst surface (Fig. 4(a) and (b)). The average size of 5 nm indi-cates that reduction at 423 K does not induce significant sintering of the particles in Cu/Pd (423) sample (Fig. S4(a) and Table 1). The average size of particles in Cu/Pd (423) sample in comparison with Pd (423) sample is decreasing by about 3 nm. The same decrease in particles size was observed by Di et al. for Pd–Cu/Al$_2$O$_3$ catalyst prepared by simultaneous reduction of Pd(NO$_3$)$_2$ and Cu(NO$_3$)$_2$ and it was explained by formation of alloy particles [2].

According to TEM–EDS measurements (Table 1), about 95% of particles in the Cu/Pd (423) catalyst are bimetallic and the average Pd and Cu contents in these particles are about 48 and 52 at%. The lattice spacing for the (200) and (111) planes, visible on the surface of these particles, is 1.87 and 2.16 Å, respectively (Fig. 4(b)). The calculated FCC lattice constant is 3.74 Å, which is between those of the Pd and Cu, suggesting the possibility of an alloy formation after catalyst reduction at 423 K. This suggestion is strengthened by the fact that the value of 2.16 Å for the (111) plane of a Cu/Pd particle in

Table 1

Structure and activity for the mono- and bimetallic catalysts. D is the average particles size measured by TEM; [AL] is the relative content of alloy particles calculated from TEM–EDS; [Cu] and [Pd] are the average metal contents in bimetallic particles calculated from TEM–EDS; $[Cu^0 + Cu^{2+}]$, $[Cu^{2+}]$, $[Pd^0]$, and $[Pd^{2+}]$ are the relative contents of Cu and Pd species calculated from XPS spectra; T_{10} is the temperature at 10% CO conversion.

Catalyst	Morphological features				Electronic features				Activity
	D nm	[AL] %	[Cu] at%	[Pd] at%	$[Cu^0 + Cu^+]$ at%	$[Cu^{2+}]$ at%	$[Pd^0]$ at%	$[Pd^{2+}]$ at%	T_{10} K
Cu (423)	4	0	0	0	43	57	0	0	510
Cu (473)	4.5	0	0	0	77	23	0	0	468
Pd (423)	8	0	0	0	0	0	78	22	448
Pd (473)	14	0	0	0	0	0	95	5	465
Cu/Pd (423)*	4	0[a]	50[a]	50[a]	34	66	0	100	477
Cu/Pd (423)	5	95	48	52	75	25	55	45	323
Cu/Pd (473)	5	74	50	50	78	22	55	45	370
Cu/Pd (523)	9	46	42	58	82	18	70	30	398
Cu/Pd (573)	14	25	30	70	86	14	80	20	419

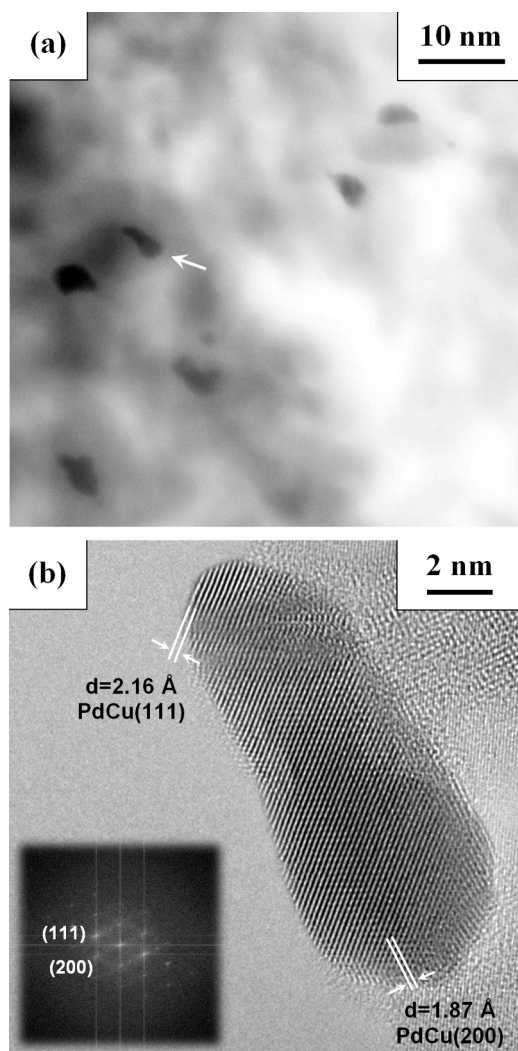[a] Ninety five percent of particles consist of a mixture of CuO and PdO; no alloy structure is formed.

Fig. 4. (a) TEM image of the particles in the Cu/Pd catalyst reduced at 423 K; (b) HRTEM image of the particle selected on TEM image and FFT pattern of this particle.

Fig. 5. (a) TEM image of the particles in the Cu/Pd catalyst reduced at 523 K; (b) HRTEM image of the particles selected on TEM image and d-spacing calculated for these particles.

the Cu/Pd (423) catalyst is in a good agreement with those reported for Pd–Cu nanoalloy particles [39–41].

The basic morphological features of the Cu/Pd (473) catalyst are similar to those of the Cu/Pd (423) catalyst: most bimetallic particles are of irregular shape and their average size is about 5 nm; the Cu/Pd ratio in bimetallic particles is 50 at%/50 at%; the lattice spacings for the (200) and (111) planes visible in the bimetallic par-
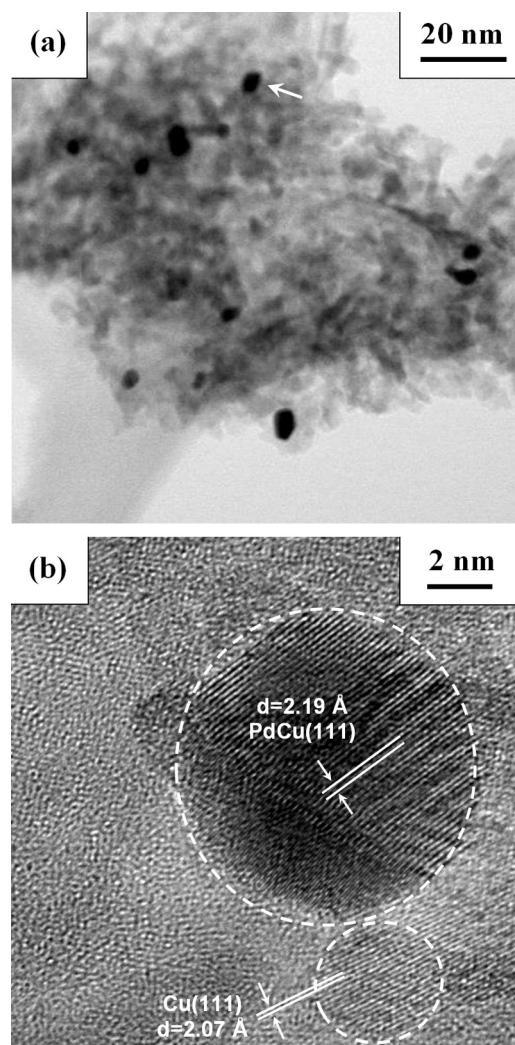
ticles are about 1.87 and 2.16 Å (Fig. S5(a) and (b)). The calculated FCC lattice constant is close to 3.74 Å. The main difference between the Cu/Pd (423) and Cu/Pd (473) catalysts is a decrease in the relative content of alloy particles: 95% in the Cu/Pd (423) catalyst vs 74% in the Cu/Pd (473) catalyst (Table 1). This indicates that reduction of Cu/Pd catalyst at 473 K results in segregation of metals in some alloy particles and formation of individual Pd and Cu particles.
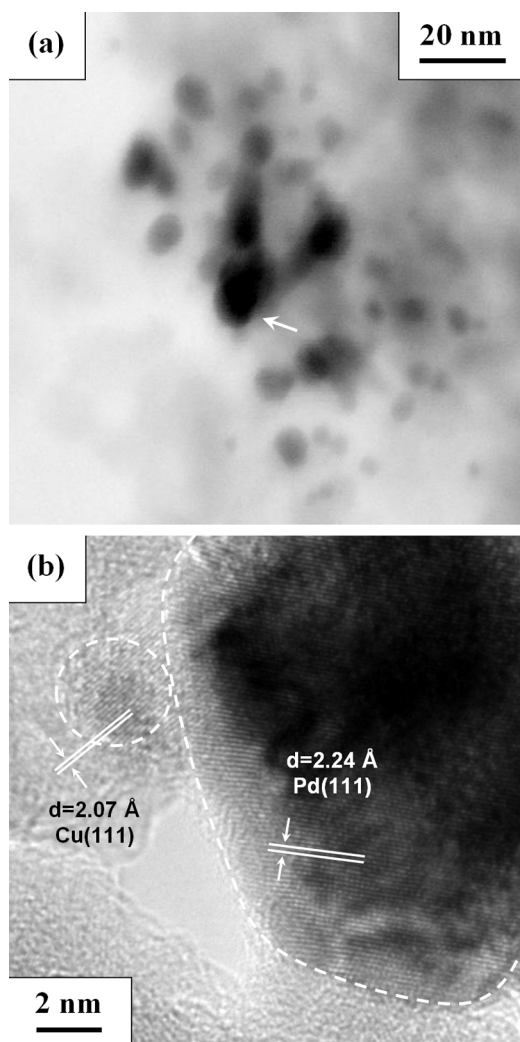
Fig. 6. (a) TEM image of the particles in the Cu/Pd catalyst reduced at 573 K; (b) HRTEM image of the particles selected on TEM image and d-spacing calculated for these particles.

Fig. 7. Cu 2p XPS spectra of the Cu, Pd, and Cu/Pd catalysts.

The segregation becomes more pronounced for the Cu/Pd catalysts reduced at 523 and 573 K. This statement follows from the decrease in the relative content of alloy particles in the Cu/Pd (523) and Cu/Pd (573) catalysts down to 46–25%, respectively (Table 1). The Pd:Cu ratio in the remaining alloy particles in the Cu/Pd catalysts reduced at 523 and 573 K becomes higher in comparison with the equimolar metal ratio observed in Cu/Pd (423) or Cu/Pd (473) samples. The lattice spacing for (111) plane in the alloy particles of Cu/Pd (523) and Cu/Pd (573) increases (Figs. 5(b) and 6(b)) and becomes close to that for metallic Pd (Fig. 2(b)). These data indicate that copper species leave the alloy particles upon high-temperature reduction. As a results a large amount of individual Pd and Cu particles are formed and the average particle size of Cu/Pd (523) and Cu/Pd (573) samples increases (Table 1). An increase of particle size in Cu/Pd (523) and Cu/Pd (573) sample can be explained by sintering of free palladium particles into large clusters (Figs. 5(a), (b), 6(a), (b), and S4(b)).

3.3. XPS measurements

3.3.1. Electronic features of copper species in catalysts

The Cu 2p XPS spectrum of the Cu (423) catalyst exhibits a doublet of Cu $2p_{3/2}$ and Cu $2p_{1/2}$ peaks at 932.8 and 952.6 eV (Fig. 7). The maximum of the Cu $2p_{3/2}$ peak for the Cu (423) sample is close
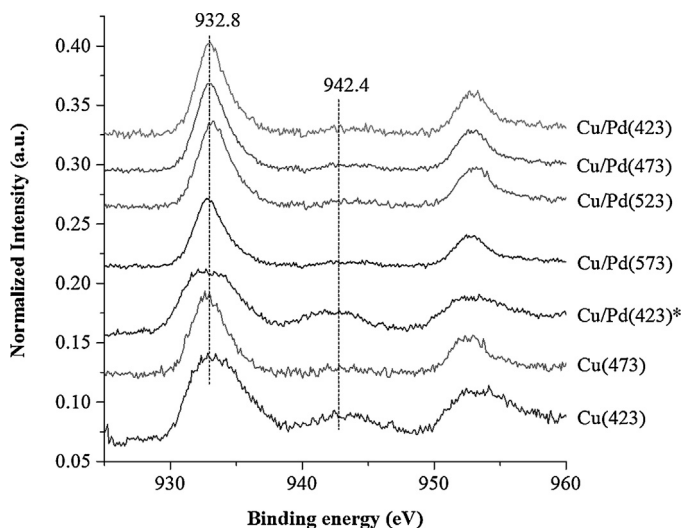
to 932.7 eV. This value can be attributed to a mixture of $Cu^0 + Cu^+$ species in supported 3–8 nm particles [42,43]. A shake-up satellite at 942.4 eV observed for the Cu (423) sample is a unique feature of Cu^{2+} spectrum and is absent in the spectra of Cu^+ and Cu^0 [35]. The precise quantification of Cu^0, Cu^+, and Cu^{2+} species from XPS spectra is always a difficult task, because of the small difference between the Cu 2p binding energies for Cu^0 and Cu^+ [44]. The Auger parameters are used widely for quantification of Cu^0, Cu^+, and Cu^{2+} species. But our situation is complicated by low intensity of Cu $L_3M_{45}M_{45}$ spectra of the catalysts, and, hence, impossibility to calculate Auger parameter for Cu species.

Nevertheless, $[Cu^0 + Cu^+]$ and $[Cu^{2+}]$ contents can be roughly estimated. Biesinger et al. reported that the area of Cu^{2+} satellite is twice lower than the area of Cu $2p_{3/2}$ peak for the Cu^{2+} species [35]. Bearing this in mind, the Cu $2p_{3/2}$ peak for the Cu (423) sample was decomposed into two components corresponding to $Cu^0 + Cu^+$ and Cu^{2+} species (Fig. S6). The analysis of component areas indicates that the $[Cu^0 + Cu^+]$ and $[Cu^{2+}]$ content in the Cu (423) sample is 43 and 57 at%, respectively (Table 1).

The Cu 2p XPS spectrum of the Cu (473) catalyst is similar to that observed for Cu (423) with the exception of decreased area of a shake-up satellite at 942.4 eV (Fig. 7). These data are indicative of a lower content of Cu^{2+} species in the Cu (473) catalyst that has been reduced at a higher temperature. Decomposition of the Cu $2p_{3/2}$ peak for Cu (473) with application of fitting procedure already used for the Cu (423) sample show that the $[Cu^0 + Cu^+]$ and $[Cu^{2+}]$ contents are 77 and 23 at% (Table 1).

The Cu 2p XPS spectrum of the unreduced Cu/Pd (423)* catalyst is presented in Fig. 7. It exhibits a doublet of Cu $2p_{3/2}$ and Cu $2p_{1/2}$ peaks at 932.7 and 952.5 eV and a pronounced shake-up satellite at about 942 eV. The calculated $[Cu^0 + Cu^+]$ and $[Cu^{2+}]$ content in this sample is 34 and 66 at%, respectively (Table 1).

The Cu 2p XPS spectrum of Cu/Pd (423) catalyst is presented in Fig. 7. The calculated $[Cu^0 + Cu^+]$ and $[Cu^{2+}]$ content in this sample is presented in Table 1. Note, the $[Cu^{2+}]$ content in Cu/Pd (423) catalyst decreases by 32 at% in comparison with the Cu (423) analog. The decreased content of Cu^{2+} species in Cu/Pd (423) catalyst could be related to a large amount of alloy particles (see Section 3.2). It is known that interaction between metal species in bimetallic alloy can change their electronic structure and modify redox properties [7,8]. We can suppose that the transfer of electrons from palladium to copper oxides on Pd^0–CuO_x interfaces is carried out. Concerning Cu/Pd (423) catalyst this should result in the weakening of Cu—O bond in copper oxides and raising the reducibility of copper oxides.
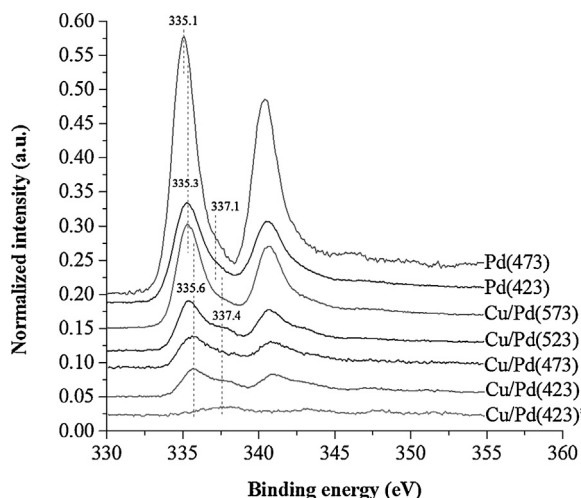
Fig. 8. Pd 3d XPS spectra of the Cu, Pd, and Cu/Pd catalysts.

Fig. 9. C 1s XPS spectra of the Cu, Pd, and Cu/Pd catalysts.

The Cu 2p XPS spectra of Cu/Pd catalyst reduced at 473–523 K are presented in Fig. 7. The calculated $[Cu^0 + Cu^+]$ and $[Cu^{2+}]$ contents are presented in Table 1. According to XPS data, increasing the reduction temperature from 423 to 573 K results in an expected decrease in the $[Cu^{2+}]$ content in Cu/Pd samples from 25 to 14 at% and a corresponding increase in the $[Cu^0 + Cu^+]$ content from 75 to 86 at% (Table 1).

3.3.2. Electronic features of palladium species in catalysts

The Pd 3d XPS spectrum of the Pd (423) catalyst exhibits a doublet of Pd $3d_{5/2}$ and Pd $3d_{3/2}$ peaks at 335.3 and 340.6 eV (Fig. 8). The maximum for Pd $3d_{5/2}$ peak can be assigned to a mixture of Pd^0 and Pd^{2+} species in Pd nanoparticles supported on alumina [36,37,45]. With the assumption of this basic model, the Pd 3d spectrum of the Pd (423) catalyst was decomposed into Pd^0 and Pd^{2+} components (Fig. S7). The calculated $[Pd^0]$ and $[Pd^{2+}]$ contents in Pd (423) are 78 and 22 at%. Increasing the reduction temperature for the Pd (473) catalyst results in an increase in the Pd^0 content up to 95 at% (Table 1).

The Pd 3d XPS spectrum of the Cu/Pd (423)* catalyst exhibits Pd $3d_{5/2}$ and Pd $3d_{3/2}$ peaks at 337.4 and 342.7 eV (Fig. 8). Ivanova et al. [36] attributed these values to PdO nanoparticles supported on alumina; hence, the $[Pd^{2+}]$ content in this sample is 100 at%.

An interesting feature of the Pd 3d XPS spectra of bimetallic catalysts in comparison with palladium samples is a low intensity of Pd 3d peaks (Fig. 8). Similar results were obtained by Di et al. [2]. Concerning unreduced Cu/Pd (423)* sample, the low intensity of Pd 3d peaks could be explained by bimetallic phases consisting of Pd^{2+} species covered with Cu^{2+} species (see Sections 3.2 and 2.1). Obviously, this external layer of Cu^{2+} species should serve as a trap for Pd^{2+} photoelectrons. In the case of reduced Cu/Pd samples, the low intensity of Pd 3d peaks could be associated with the presence of the M^{n+} species and/or the formation of Cu/Pd alloy particles with specific structure.

Another interesting feature of Cu/Pd catalysts is the shift of Pd 3d peaks to higher energy in comparison with the position of Pd 3 d peaks recorded for Pd analogs. This shift is more pronounced for the Cu/Pd (423) sample with the particles size of 5 nm and is less pronounced for Cu/Pd (573) sample with the particles size of 14 nm. The positive shift of Pd 3 d peaks for small metal clusters in XPS spectra is a common phenomenon and is related to the final-state effects [36]. Strong interaction between Pd and Cu in the alloy particles may also contribute to the positive shift of Pd 3 d peaks due to the initial-state effects [2,36].
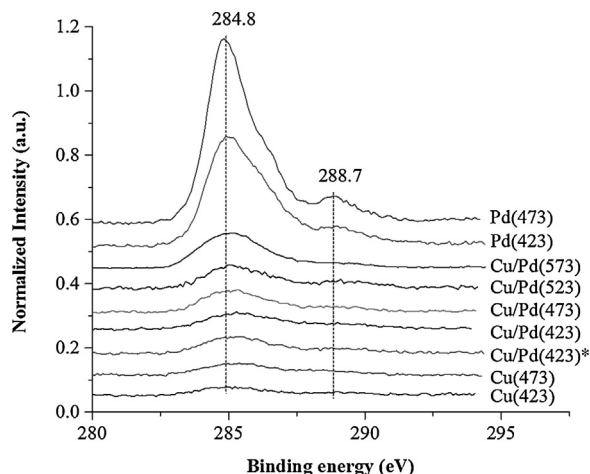
Assuming the maximum of Pd 3d low-energy component to be due to Pd^0, we can apply the fitting procedure already used for monometallic Pd catalyst and find the $[Pd^0]$ and $[Pd^{2+}]$ contents. These values are presented in Table 1 and indicate that increasing the reduction temperature from 423 to 573 K results in an expected increase in the $[Pd^0]$ content and the corresponding decrease in the $[Pd^{2+}]$ content in Cu/Pd catalysts.

Note that the $[Pd^{2+}]$ content in the Cu/Pd (423) catalyst is higher than that in the reduced Pd (423) analog: 45% vs 22% (Table 1). The observed phenomenon could be explained by interactions between metal species and modification of their redox properties. We have already observed such a modification for CuO_x species in Cu/Pd catalysts (Section 3.3.1). According to Cu/Pd catalysts, it seems that interaction between metal species on bimetallic interfaces strengthens Pd–O bond and decreases the reducibility of PdO species.

If this suggestion is right then we should see the inverse relationship between the content of alloy particles and the $[Pd^{2+}]$ content. And it is observed: $[Pd^{2+}]$ content in the Cu/Pd (423) catalyst with a high number of alloy particles (a high concentration of bimetallic interfaces) is 45%; $[Pd^{2+}]$ content in the Cu/Pd (473) catalyst with an average number of alloy particles is 30%. $[Pd^{2+}]$ content in the Cu/Pd (573) catalyst with a small number of alloy particles is 20%.

3.3.3. Adsorption of RH and CO species

The C 1s XPS spectra are presented in Fig. 9. The peak at 284.8 eV is attributable to RH species that were adsorbed from air during preparation of the catalysts. RH species are always present in real catalysts, covering their surface and reducing the activity. The intensity of the 284.8 eV peak varies in the series: Cu (423) < Cu (473) < Cu/Pd (423)* ≈ Cu/Pd (423) ≈ Cu/Pd (473) < Cu/Pd (523) < Cu/Pd (573) < < Pd (423) < Pd (473). This result indicates that adsorption of RH species on alloy particles is suppressed as compared with the Pd particles.

The shoulder peak at about 288.7 eV visible in the C 1s XPS spectra is attributable to CO molecules [44,46] adsorbed from air during preparation of the catalysts. This peak appears only in the spectra of reduced Pd (423) and Pd (473) samples; this is in line with the data about strong adsorption of CO on metallic palladium [47,48]. No peaks at about 288.7 eV are observed in the spectra of reduced Cu samples; this is in line with weak and reversible adsorption of CO on metallic copper [44]. Cu/Pd samples exhibit low-intensity peak at about 288.7 eV, indicating a decreased CO adsorption from the environment in bimetallic samples in comparison with monometallic Pd samples (Fig. 9).
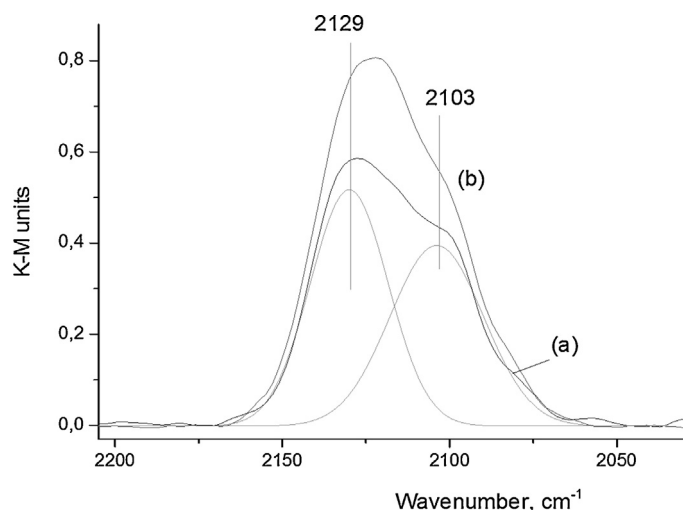
Fig. 10. DRIFT spectra of CO adsorbed on the Cu samples at RT and equilibrium pressure of 0.2 kPa: (a) Cu (423) catalyst; (b) Cu (473) catalyst.
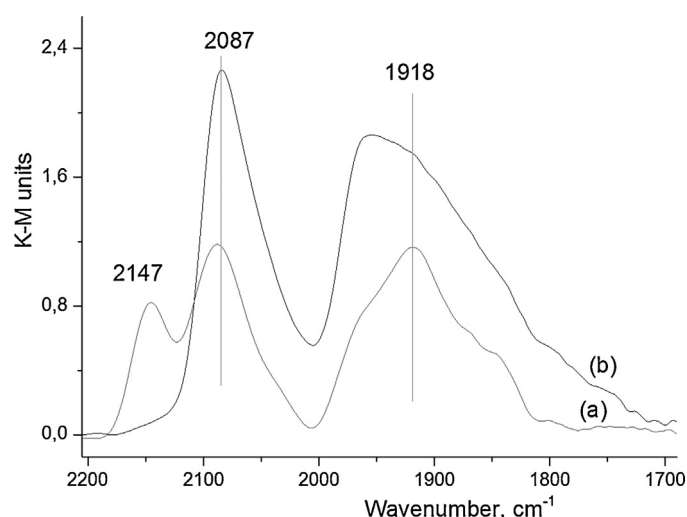

Fig. 11. DRIFT spectra of CO adsorbed on the Pd samples at RT and equilibrium pressure of 0.2 kPa: (a) Pd (423) catalyst; (b) Pd (473) catalyst.

3.4. DRIFTS measurements

The probing depth of XPS analysis varies between 3 and 10 nm, depending upon the material and the kinetic energy of photoelectrons [49,50]. The average size of metal particles in our catalysts is 4–14 nm; hence, XPS data concerning the electronic features of Cu and Pd should be assigned to the "surface + bulk" atoms of particles. DRIFTS analysis provides information about the electronic features of Cu and Pd in upper layers of particles; thus, DRIFTS results should be assigned to "surface" atoms in particles. According to this point of view, XPS and DRIFTS measurements complement each other and help us to understand the dimensional distribution of metal species in different oxidation states in supported particles.

3.4.1. Cu and Pd catalysts

The adsorption of CO on the Cu (423) and Cu (473) catalysts produces two overlapping bands at 2103 and 2129 cm^{-1} (Fig. 10(a) and (b)). These bands are assignable to Cu^0–CO and Cu^+–CO carbonyls [42,51]. No bands for Cu^{2+}–CO carbonyls in the 2150–2190 cm^{-1} range [52,53] were detected. Note that XPS spectra show the presence of Cu^{2+} species in Cu samples reduced at 423–473 K (Table 1). Such a "contradiction" between DRIFTS and XPS results is resolved in a simple assumption that the particles in our Cu catalysts consist of the surface Cu^0 and Cu^+ species located on the nuclei of unreduced Cu^{2+} species.

The DRIFT spectra of Cu catalysts were decomposed into Cu^0 and Cu^+ components and the surface content of Cu^0 and Cu^+ species was calculated from peak areas as described by Davydov [53]. The $[Cu^0]_{surf}$ and $[Cu^+]_{surf}$ content in Cu (423) is 74 and 26 at%. The $[Cu^0]_{surf}$ and $[Cu^+]_{surf}$ content in Cu (473) is 87 and 13 at%.

The DRIFT spectra of Pd catalysts are presented in Fig. 11(a) and (b). The bands at 1918 and 2087 cm^{-1} are assignable to bridge- and linearly-bonded Pd^0–CO carbonyls [54]. The band at 2147 cm^{-1} is assignable to Pd^{2+}–CO carbonyls [53].

Combining DRIFTS and XPS data (Fig. 11(a) and Table 1), we can propose that particles in the Pd (423) sample consist of surface $Pd^0 + Pd^{2+}$ species located on the nuclei of Pd^{2+} species. The precise quantification of the surface contents of Pd^0 and Pd^{2+} species from DRIFT spectrum of Pd (423) catalyst is a difficult task, because of the complex shape of peaks attributable to Pd^0–CO carbonyls. The reduction of Pd catalyst under H_2 at 473 K results in disappearance of 2147 cm^{-1} band and in increasing the intensity of bands at about 1918 and 2087 cm^{-1} (cf . Fig. 11(a) and (b)). These data can be interpreted as complete reduction of the surface Pd^{n+} atoms
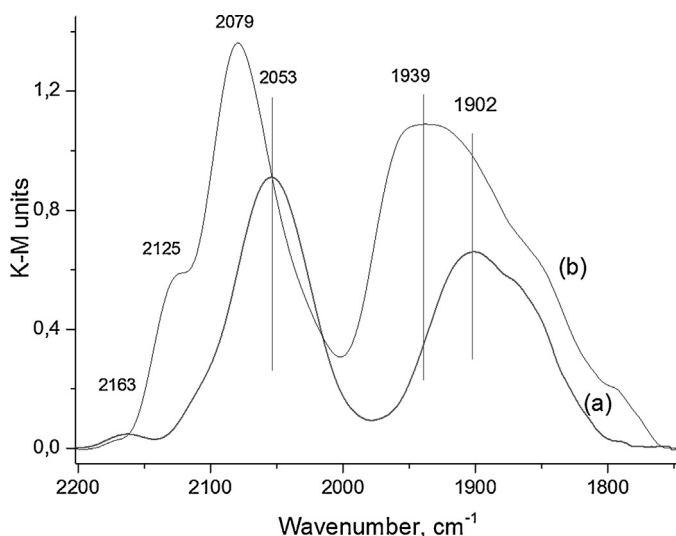

Fig. 12. DRIFT spectra of CO adsorbed on the Cu/Pd samples at RT and equilibrium pressure of 0.2 kPa: (a) Cu/Pd (423) catalyst; (b) Cu/Pd (573) catalyst.

of the Pd (473) catalyst after its treatment with H_2 at 473 K. This statement is in good agreement with XPS results that show 95% of palladium atoms in the Pd (473) catalyst to be in the zero-valence state (Table 1).

The relative amount of CO adsorbed on the surface of Cu and Pd catalysts can be calculated from intensity of peaks and IR extinction coefficients for the adsorbed M–CO carbonyls [53]. But we can use a quick estimation [53] based on the intensity of a band at about 2100 cm^{-1}, which is corresponded to linearly bonded M–CO carbonyls (Figs. 10(a), (b), 11(a), and (b)). The intensity of this band varies in the series: Cu (423) < Cu (473) and Pd (423) < Pd (473). The obtained correlations are in agreement with those obtained from XPS C 1s spectra (Section 3.3.3) and indicate that the increase in the reductive temperature results in an increased adsorption of CO species on the monometallic catalyst.

3.4.2. Cu/Pd catalysts

The DRIFT spectrum of the Cu/Pd (423) catalyst is presented in Fig. 12(a). The interpretation of this spectrum is complicated, because both Cu^0–CO and Cu^+–CO carbonyl bands observed as small absorption shoulders at about 2100–2120 cm^{-1} are disguised

by intense band of linearly bonded Pd^0–CO carbonyls. Moreover, band at about 2163 cm^{-1} visible in the DRIFT spectrum can be associated with Pd^{2+}–CO and/or Cu^{2+}–CO carbonyls.

The most interesting information that can be obtained from the spectrum of Cu/Pd (423) catalyst is concerned with the frequencies of bands assignable to Pd^0-carbonyls. The frequency of the band assignable to linearly bonded Pd^0–CO carbonyls in the spectrum of Cu/Pd (423) is 2053 cm^{-1}, which is about 34 cm^{-1} lower than that recorded for the Pd (423) catalyst. The band assignable to bridge-bonded Pd^0-carbonyls in the spectrum of Cu/Pd (423) also moves to lower frequencies: from 1918 to about 1902 cm^{-1} (Figs. 11(a) and 12(a)). These spectral features of the Cu/Pd (423) sample could be related to formation of an alloy with lattice parameters that differ from the lattice parameters of pure Pd or Cu. The phenomena of this type are widely discussed in Ref. [7–9].

Also, DRIFT spectra presented in Fig. 11(a) and 12(a) illustrate that the intensity of the bands corresponded to Pd^0–CO carbonyls for the Cu/Pd (423) sample in comparison with its monometallic Pd (423) analog decreases. This result indicates that the adsorption of CO molecules on alloy particles is suppressed. The similar conclusion was obtained from XPS C 1s spectra of the corresponded catalysts (Section 3.3.3, Fig. 9, Cu/Pd (423) and Pd (423)).

The DRIFT spectrum of the Cu/Pd (573) catalyst is presented in Fig. 12(b). Comparison of this spectrum with that recorded for the Cu/Pd (423) catalyst indicates that heating of Cu/Pd catalyst under H_2 in the range of 423–573 K results in disappearance of the band at about 2163 cm^{-1} and appearance of a band at about 2125 cm^{-1}, indicating the reduction of surface M^{2+} species to M^+ species. The DRIFTS data are in agreement with XPS data (Table 1). The reduction of the Cu/Pd (573) catalyst under H_2 at 573 K is also accompanied by decreasing CO frequency in Pd^0-carbonyls in comparison with that observed in the spectra of Pd catalysts (Figs. 12(b), Fig. 11(a) and (b)). However, the shifts of the corresponding ν CO-bands in the spectrum of the Cu/Pd (573) catalyst is significantly smaller than these shifts in the spectrum of Cu/Pd (423). For example, the CO frequencies in linearly bonded Pd^0–CO carbonyls in the spectra of Pd (473), Cu/Pd (573), and Cu/Pd (473) are 2087, 2079, and 2053 cm^{-1}, respectively. This result can be explained by segregation of alloy particles in Cu/Pd catalysts under reduction at high temperature and is in good agreement with TEM–EDS–FFT data discussed in Section 3.2.

Finally, it should be mentioned that the intensity of the bands corresponded to Pd^0–CO carbonyls for the Cu/Pd (573) sample in comparison with the Cu/Pd (423) catalyst increases. This indicates that the adsorption of CO molecules on Cu/Pd (573) is enhanced. The enhanced adsorption of CO on Cu/Pd (573) catalyst can be explained by segregation of alloy particles, that results in the strong adsorption of CO molecules on individual Pd^0 particles. As a result the adsorptive properties of Cu/Pd (573) sample become more similar with that of Pd samples.

3.5. CO oxidation

In order to suppress the possible modification of our samples during catalysis, the pulsed micro catalytic method with a dilute reactant mixture was applied in this study. The results of catalytic experiments are presented in Fig. 13(a) and (b).

Fig. 13(a) shows the plot for CO conversion vs the number of reaction mixture pulses for mono- and bimetallic samples at 448 K. This temperature is higher than a common temperature required for low-temperature CO oxidation, i.e., at about 350 K. It can be seen that CO conversion on catalysts does not depend on the pulse number (Fig. 13(a)). These results imply that the number of active sites of different types on the surface of catalysts remains unchanged during CO oxidation carried out at temperatures below 448 K.
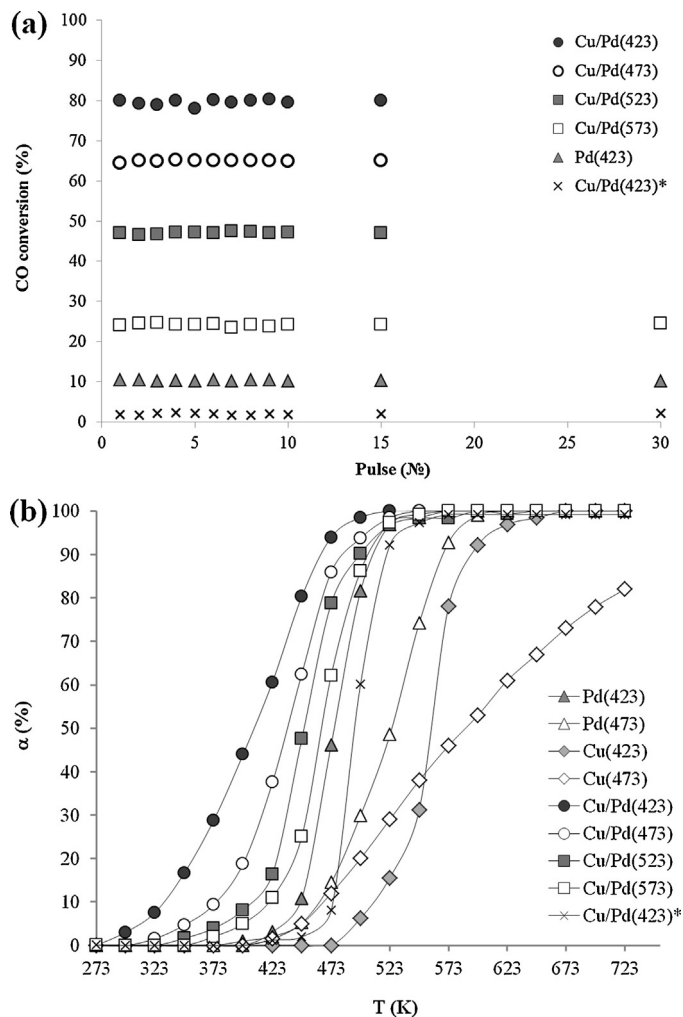

Fig. 13. (a) CO conversion over Pd and Cu/Pd catalysts at 448 K as a function of pulse number; (b) steady-state CO conversion (α) over the Cu, Pd, and Cu/Pd catalysts as a function of reaction temperature (T).

This statement is also confirmed by XPS and TEM studies of the catalysts after reaction at 448 K (not presented), which show the identity of catalyst structure before and after the reaction. Consequently, the differences in catalyst activity measured in the range of 273–448 K can be interpreted with application of the original structure discussed earlier in Sections 3.1–3.4.

3.5.1. CO oxidation over Cu and Pd catalysts

The oxidation of CO on the Cu (423) and Cu (473) sample starts at about 475 and 448 K, respectively (Fig. 13(b)). The values of T_{10} for Cu (423) and Cu (473) samples are 510 and 468 K, respectively (Table 1). The difference in the light-off activity of Cu catalysts cannot be explained by morphology features, because both Cu catalysts have almost similar particle size distributions and similar particle shape. However, the high light-off activity of Cu (473) in comparison with Cu (423) can be explained by conversion of Cu^{2+} to Cu^0 and Cu^+, which proceeds vigorously during the reduction of Cu catalyst with H_2 at 473 K (Table 1).
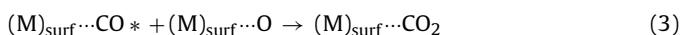
This explanation is in a good agreement with results published in Ref. [55,56]. Huang et al. compared the activities of Cu, Cu_2O, and CuO powders toward CO oxidation with O_2 [55]. The CO conversions at 413 K in the presence of Cu_2O, CuO, or Cu were found to be 80, 0.1, and 0.2%, respectively. The reaction follows Mars van Krevelen (MvK) mechanism described in Ref. [16,55]. White et al.

studied CO oxidation catalyzed by Cu_2O and CuO powders [56]. At 453 K, the activity was found to vary in the order: $Cu_2O > CuO$.

CO oxidation on the Pd (423) and Pd (473) samples starts at 400 and 423 K, respectively (Fig. 13(b)). The different particle size was observed for these catalysts (Table 1), but, in our opinion, the difference in the activity of Pd catalysts cannot be explained by these features, because the light-off activity of Pd catalysts does not depend strongly on the Pd particle size. Herein we refer to Ivanova et al. [36]. They compared the activities of Pd particles supported on Al_2O_3 toward CO oxidation with O_2 [36]. The values of T_{10} for the supported Pd particles with the size of 3, 4, and 7 nm were found to be 405, 405, and 410 K, respectively.

In our opinion, the main difference in the light-off activity of the Pd (423) and Pd (473) catalysts can be explained by differences in the electronic states of Pd species and their adsorptive properties. Herein, some known facts should be given first. It is accepted that CO oxidation on platinum metals follows the Langmuir–Hinshelwood (L–H) mechanism [16].

The catalytic cycle of L–H oxidation of CO on metal surface $(M)_{surf}$ comprises: dissociative adsorption of O_2, Eq. (1); CO adsorption and activation, Eq. (2); reaction of O atom with activated CO* molecule, Eq. (3); and CO_2 desorption to the gas phase, Eq. (4).

$$(M)_{surf} + \tfrac{1}{2}O_2 \rightarrow (M)_{surf} \cdots O \qquad (1)$$

$$(M)_{surf} + CO \rightarrow (M)_{surf} \cdots CO* \qquad (2)$$

$$(M)_{surf} \cdots CO* + (M)_{surf} \cdots O \rightarrow (M)_{surf} \cdots CO_2 \qquad (3)$$

$$(M)_{surf} \cdots CO_2 \rightarrow (M)_{surf} + CO_2 \qquad (4)$$

According to the L–H mechanism, the low rate of CO oxidation at 273–423 K is explained by the preferential adsorption of CO molecules on Pd^0 species (Eq. (2)) that prevents further dissociation of O_2 molecules on these catalytic sites [16]. Consequently, Pd (473) sample containing almost all palladium atoms in the zero-valence state, should not be a very active catalyst. And this is correct: CO oxidation on Pd (473) sample starts at about 423 K and its light-off activity is relatively low (Table 1). In contrast with the Pd (473) sample, there are 78% of Pd^0 and 22% of PdO species on the surface of Pd (423). It is known that palladium oxides can serve as a supplier of active oxygen atoms for oxidation of adsorbed CO molecules [16]. This implies the conversion of CO molecules strongly bound to Pd^0 to CO_2 molecules on Pd^0–PdO interface, which are desorbed from the surface. As a result, a part of "blocked" Pd^0 atoms in the Pd (423) catalyst becomes available for adsorption and dissociation of O_2 molecules. This should be favorable for low-temperature CO oxidation on Pd^0 atoms via L–H mechanism. Note, that the surface of as prepared Pd samples is covered with CO molecules adsorbed on some Pd^0 sites from the environment. In the case of Pd (423) sample, adsorption of CO molecules is somewhat suppressed (Sections 3.3.3 and 3.4.1), which is in agreement with the explanations presented above.

3.5.2. CO oxidation over Cu/Pd catalysts

CO oxidation on the Cu/Pd (423)* sample starts at about 433 K (Fig. 13(b)). The T_{10} value for this sample is 477 K. The low activity of Cu/Pd (423)* can be explained by the absence of Pd^0 sites, which are necessary for dissociative adsorption of O_2 (Eq. (1)).

The oxidation of CO on the Cu/Pd (423) sample starts at about 275 K (Fig. 13(b)). The T_{10} value for this sample is 323 K. Comparison of T_{10} for Cu/Pd (423), Pd (423), and Cu (423) indicates a synergy between metal species in the Cu/Pd catalyst, resulting in a remarkable increase of activity.

There are structural features of Cu/Pd (423) sample that can be responsible for the synergistic effect. First of all, there is an increased content of Pd^{2+} and essential amount of Pd^0 in the Cu/Pd (423) catalyst. So, we could propose the formation of Pd^0–PdO

interfaces and enhancing of Pd^0 phase activity as described in Section 3.5.1. Note, that an increase in the $[Pd^{2+}]$ content in Pd (423) in comparison with Pd (473) catalyst by about 20% results in a decrease of T_{10} by about 20 K. But, an increase in the $[Pd^{2+}]$ content in Cu/Pd (423) in comparison with Pd (423) catalyst by about 20% results in a decrease of T_{10} by about 130 K! This means that Pd^0–PdO interfaces are not the most active sites in Cu/Pd samples. Next, an apparent activation energy for CO oxidation in the presence of the Cu/Pd (423), Pd (423), and Cu (423) catalyst is 30, 90, and 110 kJ/mol, respectively (Fig. S8). These values also indicate that CO oxidation in the presence of Cu/Pd (423) is carried out predominantly on new sites.

Ninety five percent of particles in Cu/Pd (423) catalyst are alloy particles with a specific structure (Table 1). The surface of Cu/Pd particles contains predominantly Pd^0 and Cu^0 atoms being in close contact with each other. The core of particles contains CuO_x. These features indicate a formation of inner Pd^0–CuO_x interfaces. We also saw Cu/Pd particles situated near CuO_x particles during TEM study and this indicates a formation of outer Pd^0–CuO_x interfaces. Finally, there are Cu^+ atoms on the surface of alloy particles (See DRIFTS measurements) and this means the formation of surface Pd^0–CuO_x interfaces. So, there are new sites in Cu/Pd catalysts and they are Pd^0–CuO_x interfaces.

Next, it is known that individual copper oxides possess high oxygen storage capacity [16]. Concerning the Cu/Pd (423) catalyst, the interaction between metal species results in the additional weakening of Cu—O bond (see Section 3.3.1). The high oxygen storage capacity and weakening of Cu—O bond implies fast extraction of lattice oxygen from CuO_x and fast oxidation of CO molecules strongly bonded to Pd^0, which are easily desorbed to reaction media. As a result, a substantial part of "blocked" Pd^0 atoms in the catalyst become available for adsorption and dissociation of O_2 molecules. This should be very favorable for low-temperature CO oxidation on Pd^0 atoms of Pd^0–CuO_x interfaces via L–H mechanism.

Heating of Cu/Pd catalysts under H_2 in the range of 443–573 K results in a decrease in the light-off activity (Table 1) and in an increase in the activation energy (Fig. S8). These phenomena can be explained by changes of the catalysts structure. According to Sections 3.2–3.4, an increase of the reduction temperature results in a segregation of alloy particles, reducing their content in Cu/Pd catalysts. The segregation is also accompanied by conversion of MO_x species to M^0 species. These processes imply the decreased amount of Pd^0–PdO and Pd^0–CuO_x interfaces in Cu/Pd samples; an increased CO adsorption; and, thus, a decreased light-off activity due to inhibition effect of CO molecules strongly bound to Pd^0 sites.

4. Conclusion

The Cu/Pd/Al_2O_3, Cu/Al_2O_3, and Pd/Al_2O_3 catalysts containing 0.37 wt% Cu and 0.64 wt% Pd were produced with application of deposition–precipitation and impregnation. The effect of hydrogen treatment at different temperatures on the activity of these catalysts toward low-temperature CO oxidation was studied by the pulsed micro catalytic method.

CO oxidation on Cu/Pd, Pd, and Cu catalysts reduced at 423 K starts at 275, 400, and 475 K, respectively, indicating a synergy between the metal species in the bimetallic catalyst. According to XRD, TEM, EDS, FFT, DRIFTS, and XPS studies, it was suggested that the enhanced light-off activity of the Cu/Pd catalyst reduced by H_2 at 423 K is attributable to the formation of bimetallic alloy particles with the size of 5 nm and a relatively high content of Pd^0 and MO_x species. The synergistic effect is explained by mechanism of CO oxidation on a Pd^0–MO_x interface. The increase in the reduction temperature results in a separation of alloy particles into individual metal particles. As a result, Cu/Pd catalysts reduced at high tem-

peratures are characterized with a decreased content of Pd^0–MO_x interfaces; an increased CO adsorption and thus a decreased light-off activity due to inhibition effect of CO molecules strongly bound to Pd^0 sites.

Acknowledgments

Appendix A. Supplementary data

Supplementary data associated with this article can be found, in the online version, at http://dx.doi.org/10.1016/j.apcatb.2017.02.038.

References

[1] S.A. Nikolaev, E.V. Golubina, I.N. Krotova, M.I. Shilina, A.V. Chistyakov, V.V. Kriventsov, Appl. Catal. B: Environ. 168–169 (2015) 303–312.
[2] L. Di, W. Xu, Z. Zhan, X. Zhang, RSC Adv. 5 (2015) 71854–71858.
[3] Y. Zhang, R.W. Cattrall, I.D. McKelvie, S.D. Kolev, Gold Bull. 44 (2011) 145–153.
[4] R.J.H. Grisel, K.J. Weststrate, A. Gluhoi, B.E. Nieuwenhuys, Gold Bull. 35 (2002) 39–45.
[5] R.J.H. Grisel, B.E. Nieuwenhuys, Catal. Today 64 (2001) 69–81.
[6] R. Ferrando, J. Jellinek, R.L. Johnston, Chem. Rev. 108 (2008) 846–910.
[7] J. Shi, Chem. Rev. 113 (2013) 2139–2181.
[8] A.K. Singh, Q. Xu, ChemCatChem. 5 (2013) 652–676.
[9] H.L. Jiang, Q. Xu, J. Mater. Chem. 21 (2011) 13705–13725.
[10] A. Wang, X.Y. Liu, C.Y. Mou, T. Zhang, J. Catal. 308 (2013) 258–271.
[11] O.G. Ellert, M.V. Tsodikov, S.A. Nikolaev, V.M. Novotortsev, Russ. Chem. Rev. 83 (2014) 718–732.
[12] S.A. Nikolaev, V.V. Smirnov, Catal. Today 147S (2009) S336–S341.
[13] S.A. Nikolaev, D.A. Pichugina, D.F. Mukhamedzyanova, Gold Bull. 45 (2012) 221–231.
[14] X. Liu, A. Wang, X. Wang, C.Y. Mou, T. Zhang, Chem. Commun. 27 (2008) 3187–3189.
[15] M.A. Centeno, K. Hadjiivanov, Tz. Venkov, Hr. Klimev, J.A. Odriozola, J. Mol. Catal. A: Chem. 252 (2006) 142–149.
[16] S. Royer, D. Duprez, ChemCatChem. 3 (2011) 24–65.
[17] X.D. Hou, Y.Z. Wang, Y.X. Zhao, Catal. Lett. 123 (2008) 321–326.
[18] Y. Lou, L. Wang, Z. Zhao, Y. Zhang, Z. Zhang, G. Lu, Y. Guo, Y. Guo, Appl. Catal. B: Environ. 146 (2014) 43–49.
[19] Y. Lou, X.M. Cao, J. Lan, L. Wang, Q. Dai, Y. Guo, J. Ma, Z. Zhao, Y. Guo, P. Hu, G. Lu, Chem. Commun. 50 (2014) 6835–6838.
[20] Y. Lou, J. Ma, X. Cao, L. Wang, Q. Dai, Z. Zhao, Y. Cai, W. Zhan, Y. Guo, P. Hu, G. Lu, Y. Guo, ACS Catal. 4 (2014) 4143–4152.
[21] K.I. Choi, A. Vannice, J. Catal. 127 (1991) 465–488.
[22] K.I. Choi, A. Vannice, J. Catal. 127 (1991) 489–511.
[23] F. Wang, H. Zhang, D. He, Environ. Technol. 35 (2014) 347–354.
[24] F. Wang, K. Zhao, H. Zhang, Y. Dong, T. Wang, D. He, Chem. Eng. J. 242 (2014) 10–18.
[25] Y. Shen, G. Lu, Y. Guo, Y. Wang, Chem. Commun. 46 (2010) 8433–8435.
[26] Y. Shen, G. Lu, Y. Guo, Y. Wang, Y. Guo, X. Gong, Catal. Today 175 (2011) 558–567.
[27] W.J. Tang, L. Zhang, G. Henkelman, J. Phys. Chem. Lett. 2 (2011) 1328–1331.
[28] S. Shan, V. Petkov, B. Prasai, J. Wu, P. Joseph, Z. Skeete, E. Kim, D. Mott, O. Malis, J. Luo, C.J. Zhong, Nanoscale 7 (2015) 18936–18948.
[29] F. Wang, G. Lu, Int. J. Hydrogen Energy 35 (2010) 7253–7260.
[30] P. Estifaee, M. Haghighi, N. Mohammadi, F. Rahmani, Ultrason. Sonochem. 21 (2014) 1155–1165.
[31] S.A. Nikolaev, V.V. Smirnov, A.Yu. Vasil'kov, V.L. Podshibikhin, Kinet. Catal. 51 (2010) 375–379.
[32] S.A. Nikolaev, N.A. Permyakov, V.V. Smirnov, A.Yu. Vasil'kov, S.N. Lanin, Kinet. Catal. 51 (2010) 288–292.
[33] S.A. Nikolaev, I.N. Krotova, Petrol. Chem. 53 (2013) 395–401.
[34] V.V. Smirnov, S.N. Lanin, A.Yu. Vasilíkov, S.A. Nikolaev, G.P. Muravíeva, L.A. Tyurina, E.V. Vlasenko, Russ. Chem. Bull. 54 (2005) 2286–2289.
[35] M.C. Biesinger, L.W.M. Lau, A.R. Gerson, R.St.C. Smart, Appl. Surf. Sci. 257 (2010) 887–898.
[36] A.S. Ivanova, E.M. Slavinskaya, R.V. Gulyaev, V.I. Zaikovskii, O.A. Stonkus, I.G. Danilova, L.M. Plyasova, I.A. Polukhina, A.I. Boronin, Appl. Catal. B: Environ. 97 (2010) 57–71.
[37] E.A. Lashina, E.M. Slavinskaya, N.A. Chumakova, O.A. Stonkus, R.V. Gulyaev, A.I. Stadnichenko, G.A. Chumakov, A.I. Boronin, G.V. Demidenko, Chem. Eng. Sci. 83 (2012) 149–158.
[38] E.B. Gordon, A.V. Karabulin, V.I. Matyushenko, T.N. Rostovshchikova, S.A. Nikolaev, E.S. Lokteva, E.V. Golubina, Gold Bull. 48 (2015) 119–125.
[39] J. Mao, Y. Liu, Z. Chen, D. Wang, Y. Li, Chem. Commun. 50 (2014) 4588–4591.
[40] Z.Q. Zhang, J. Huang, L. Zhang, M. Sun, Y.C. Wang, Y. Lin, J. Zeng, Nanotechnology 25 (2014), 435602(6).
[41] C. Hu, X. Zhai, Y. Zhao, K. Bian, J. Zhang, L. Qu, H. Zhang, H. Luo, Nanoscale 6 (2014) 2768–2775.
[42] Z. He, H. Lin, P. He, Y. Yuan, J. Catal. 277 (2011) 54–63.
[43] L.F. Chen, P.J. Guo, M.H. Qiao, S.R. Yan, H.X. Li, W. Shen, H.L. Xu, K.N. Fan, J. Catal. 257 (2008) 172–180.
[44] T. Ghodselahi, M.A. Vesaghi, A. Shafiekhani, A. Baghizadeh, M. Lameii, Appl. Surf. Sci. 255 (2008) 2730–2734.
[45] Y. Zhang, Y. Cai, Y. Guo, H. Wang, L. Wang, Y. Lou, Y. Guo, G. Lu, Y. Wang, Catal. Sci. Technol. 4 (2014) 3973–3980.
[46] N. Schumacher, K. Andersson, L.C. Grabow, M. Mavrikakis, J. Nerlov, I. Chorkendroff, Surf. Sci. 602 (2008) 702–711.
[47] P.J. Berlowitz, C.H.F. Peden, D.W. Goodman, J. Phys. Chem. 92 (1988) 5213–5221.
[48] S.M. McClure, D.W. Goodman, Chem. Phys. Lett. 469 (2009) 1–13.
[49] C.J. Powell, A. Jablonski, J. Surf. Anal. 17 (2011) 170–176.
[50] S. Tanuma, T. Shiratori, T. Kimura, K. Goto, S. Ichimura, C.J. Powell, Surf. Interface Anal. 37 (2005) 833–845.
[51] Y.N. Wang, X. Duan, J. Zheng, H. Lin, Y. Yuan, H. Ariga, S. Takakusagi, K. Asakura, Catal. Sci. Technol. 2 (2012) 1637–1639.
[52] J.E. Bailie, G.J. Hutchings, H.A. Abdullah, J.A. Anderson, C.H. Rochester, Phys. Chem. Chem. Phys. 2 (2000) 283–290.
[53] A.A. Davydov, in: N.T. Sheppard (Ed.), Molecular spectroscopy of oxide catalyst surfaces, John Wiley & Sons Ltd, Chichester, England, 2003, pp. 1–668.
[54] S. Bertarione, D. Scarano, A. Zecchina, V. Johánek, J. Hoffmann, S. Schauermann, M.M. Frank, J. Libuda, G. Rupprechter, H.J. Freund, J. Phys. Chem. B 108 (2004) 3603–3613.
[55] T.J. Huang, D.H. Tsai, Catal. Lett. 87 (2003) 173–178.
[56] B. White, M. Yin, A. Hall, D. Le, S. Stolbov, T. Rahman, N. Turro, S. O'Brien, Nano Lett. 6 (2006) 2095–2098.